Proceedings of ASME Turbo Expo 2009: Power for Land, Sea and Air
GT2009
June 8-12, 2009, Orlando, Florida, USA

GT2009-59111

COMPUTATIONAL DESIGN OF CORROSION-RESISTANT FE-CR-NI-AL NANOCOATINGS FOR POWER GENERATION[1]

K. S. Chan
W. Liang
N. S. Cheruvu
Southwest Research Institute
6220 Culebra Road, San Antonio, TX 78238

D. W. Gandy
Electric Power Research Institute
Charlotte, NC 28262

ABSTRACT

A computational approach has been undertaken to design and assess potential Fe-Cr-Ni-Al systems to produce stable nanostructured corrosion-resistant coatings that form a protective, continuous scale of alumina or chromia at elevated temperatures. Phase diagram computation was modeled using the Thermo-Calc® software and database [1, 2] to generate pseudo-ternary Fe-Cr-Ni-Al phase diagrams to help identifying compositional ranges without undesirable brittle phases. Computational modeling of the grain growth process, sintering of voids, and interface toughness determination by indentation, assessed micro-structural stability and durability of the nanocoatings fabricated by a magnetron-sputtering process. Interdiffusion of Al, Cr, and Ni was performed using the DICTRA® diffusion code [3] to maximize the long-term stability of the nanocoatings.

The computational results identified a new series of Fe-Cr-Ni-Al coatings that maintain long-term stability and a fine-grained microstructure at elevated temperatures. The formation of brittle sigma phase in Fe-Cr-Ni-Al alloys is suppressed for Al contents in excess of 4 wt.%. Grain growth modeling indicated that the columnar-grained structure with a high percentage of low-angle grain boundaries is resistant to grain growth. Sintering modeling indicated that the initial relative density of as-processed magnetron-sputtered coatings could achieve full density after a short thermal exposure or heat-treatment. Interface toughness computation indicated that Fe-Cr-Ni-Al nanocoatings exhibit high interface toughness in the range of 52–366 J/m^2. Interdiffusion modeling using the DICTRA software package indicated that inward diffusion could result in substantial to moderate Al and Cr losses from the nanocoating to the substrate during long-term thermal exposures.

INTRODUCTION

Energy-producing steam and gas turbine components operate in a severe environment at elevated temperatures. For protection against environmental degradation, both MCr and MCrAl (where M = Fe, Ni, Co or combination of these elements) are widely used in industry. A large number of oxidation–resistant Ni-Cr-Al coatings are available for protection of gas-turbine protection at service temperatures up to about 1100°C [4–12]. For these Ni-based coatings, the Cr content ranges from 3 to 22 wt.% and the Al content ranges from 2–20 wt.%, with no or little Fe. Most of the Ni-Cr-Al coatings are processed using conventional methods and exhibit normal grain sizes. Recently, some investigators have processed Ni-Cr-Al coatings with a nano-scaled grain structure [4–11].

Several Fe-Cr-Ni-Al coatings with nano-scaled grain structure are also reported in the literature [13–15]. Liu et al. [14, 15] reported the oxidation characteristics of sputtered-deposited nanocrystalline Fe-Cr-Ni-Al coatings with 25–26 wt.% Cr, 19.3 wt.% Ni, and 3.4–4.2 wt.% Al, with and without 1.8 wt.% Mn. The compositions of these coatings are essentially those of 310 stainless steels (Fe-25Cr-19.3Ni) with the additions of 3.4–4.2 wt.% Al and 1.8 wt.% Mn. Nanocoatings based on 304 stainless steel compositions with 3 wt.% to 10 wt.% Al additions (Fe-18Cr-8Ni-zAl, where z ranges from 3 to 10 wt.%) were also reported [13]. By virtue of a nano-scaled grain structure, these nanocoatings are capable of forming a continuous Al_2O_3 oxide scale in 100 hours at 800 and 900°C [14], and 50 hrs at 950°–1050°C [15]. These authors did not report oxidation results for longer times of thermal exposure.

He et al. [16] reported the synthesis of micro-crystalline Fe-Cr-Ni-Al-Y_2O_3 oxide-dispersion strengthened alloy coatings by electric-spark deposition using Fe-20Cr-4.5Al-0.5Ti-0.5Y_2O_3-0.23C-0.002S (in wt.%) as an electrode and Fe-1Cr-18Ni-9Ti as the substrate. The coating produced was Fe-18.9%Cr-7.98%Ni-2.41%Al. Because of its relatively low Al content, this particular coating (Fe-18.9%Cr-7.98%Ni-2.41%Al) does not form continuous Al_2O_3, but rather forms a combination of mixed $FeCr_2O_4$ and Cr_2O_3 [16]. Thus, it is unknown whether or not that coating containing low levels of Al provides long-term protection. There are also questions about the long-term stability of the nano-sized grain structure at elevated temperature.

[1] This work is funded by DOE through Contract No. DE-FC26-07NT43096.

Since elevated-temperature tests are expensive, there is a need for an efficient approach to reduce the cost and lead time for developing novel coatings with improved oxidation and corrosion performance. One possible approach is to utilize computational methods to design and optimize the compositions and to interrogate the microstructural stability of nanostructured coatings. In this paper, we report the use of an integrated computational approach to develop a stable nanostructured coating that produces a protective, continuous scale of alumina or chromia. The computational efforts included (1) the use of Thermo-Calc® software and database [1, 2] for computing pseudo-ternary phase diagrams for the design of nanocoatings; (2) the use of grain growth model, sintering model, and interface toughness model for optimizing microstructural stability and interface integrity; and (3) the use of DICTRA diffusion code [3] for maximizing the long-term stability of the nanocoatings. The candidate nanocoatings were fabricated by a magnetron-sputtering process.

COMPUTATIONAL DESIGN OF NANOCOATING COMPOSITIONS

Pseudo-ternary phase diagrams for Fe-Cr-Ni-Al systems were computed using Thermo-Calc Windows Version 4 (TCW-4) [1] and TCFE5 [2], which is a thermodynamic database for steels and Fe-based alloys by Thermo-Calc Software. This effort was intended to provide guidance on the phase relations of both alumina and chromia formers over the operating temperature range for selected aluminum contents. The intended application of the Fe-Cr-Ni-Al coatings is fossil-fired steam turbine boilers. Since the application temperatures can range from 455°C to 750°C, the pseudo-ternary phase diagrams were computed from 327°C to 927°C at 100°C increments. The aluminum content was selected to range from 0 wt.% to 14 wt.% at 2 to 3 wt.% increments. One of the goals of the phase diagram computation is to identify the minimum amounts of Al addition required to suppress sigma phase formation in Fe-Cr-Ni-Al alloys. To achieve this goal, the Fe-Cr-Ni-Al pseudo-ternary phase diagram was computed for 727°C by increasing the Al content from 0 wt.% to 10 wt.% at 1 wt.% increments.

The computational results have been utilized to establish the minimum Al contents and temperature where σ phase would be suppressed. The results are presented in Fig. 1, which indicate that a 4 wt.% Al addition or greater suppresses the formation of σ phase in Fe-Cr-Ni-Al at 372–627°C. The amount of Al addition required to suppress σ phase formation decreases with increasing temperature to about 3 wt.% Al at 727°C and to 2 wt.% Al at 827°C, as shown in Fig. 1. At Al contents greater than 4 wt.%, the microstructures of Fe-Ni-Cr-Al contain ferrite (bcc), austenite (fcc), or a combination of ferrite + austenite. Al is a bcc stabilizer that expands the bcc phase field, but diminishes the σ phase and austenite (fcc) phase fields in Fe-Ni-Cr-Al. Typical pseudo-ternary phase diagrams for Fe-Ni-Cr-Al at 727°C are presented as a function of Al content in Fig. 2.

The general trend is that increasing Al content expands the bcc phase field and suppresses the formation σ phase. Figs. 3(a), (b), (c), and (d) present the pseudo-ternary phase diagrams for Fe-Cr-Ni-10wt.%Al for 427, 527, 627, and 827°C. The corresponding result for 727°C is shown earlier Fig. 2(d). At 700K, a phase field of two bcc phases (α_1 is Fe-rich and α_2 is Cr-rich) and one fcc phase (γ) exist in the central portion of the phase diagram. The size of this phase field diminishes at 527°C and is completely gone at 627°C. At 627°C, 727°C, and 827°C, the equilibrium phases are α (bcc) and γ (fcc).

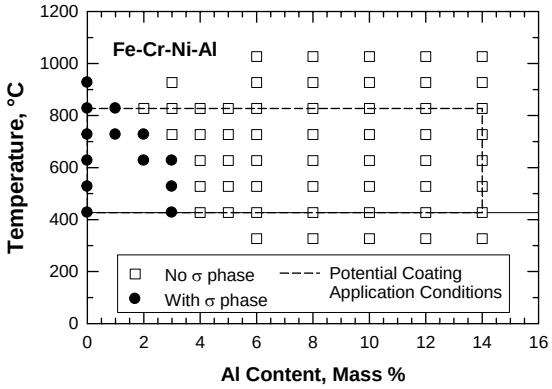

Fig. 1. Computational results of Al contents required to suppress σ-phase formation in Fe-Cr-Ni-Al at a temperature in the range of 327–1027°C.

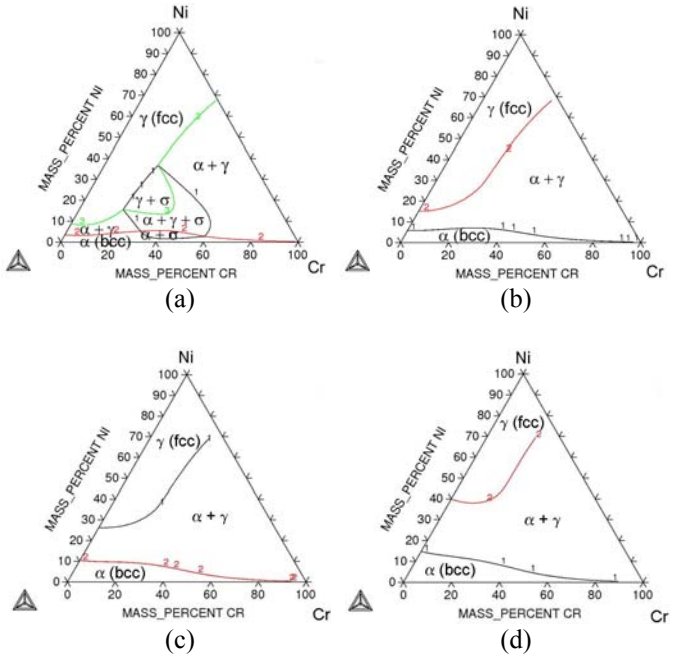

Fig. 2. Computed pseudo-ternary phase diagrams for Fe-Cr-Ni-Al alloys at 727°C: (a) 1 wt.% Al, (b) 3 wt.% Al, (c) 6 wt.% Al, and (d) 10 wt.% Al.

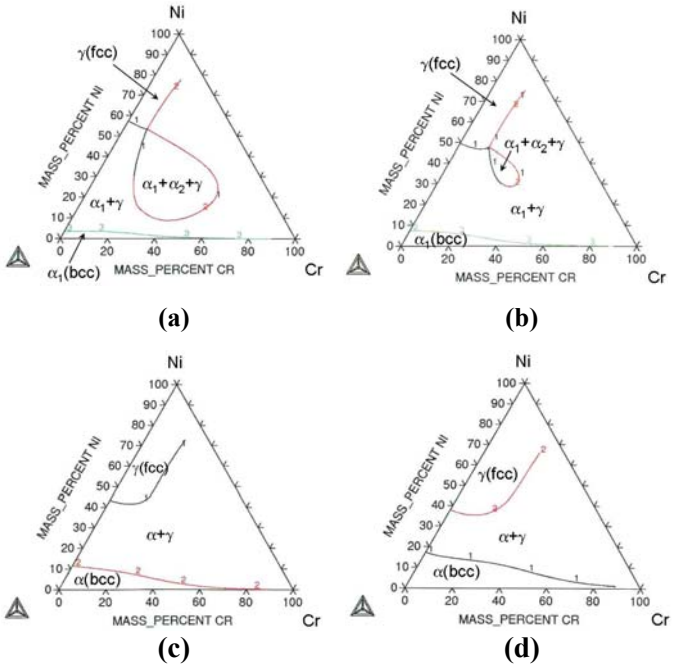

Fig. 3. Computed pseudo-ternary phase diagrams for Fe-Cr-Ni-Al alloys with 10 wt.% Al for various temperatures: (a) 427°C, (b) 527°C, (c) 627°C , and (d) 827°C .

Al contents have been reported to produce alumina formation in Fe-Ni-Cr-Al alloys [15, 17–23]. A minimum of 4 to 5 wt.% Al is required to form a continuous alumina scale on Fe-Ni-Cr-Al alloys. It has been reported that a minimum of 5 wt.% Al is required to form a continuous alumina scale on coatings with a normal grain size (> 1 μm). The critical Al content is reduced from 5 wt.% to 3.5 wt.% Al for coating with nano-sized grain size because of a greater Al diffusion kinetics through grain boundaries [15, 23]. The critical Al content for Fe-Ni-Cr-Al alloys can be further reduced to the 2.5 wt.% to 4.0 wt.% range by controlling the contents of microalloying elements such as Ti, V, and Nb [24–26]. The minimum Al content required for Al_2O_3 formation is also about 3.5 wt.% Al for aluminide coatings on Fe-based alloy substrates [27]. To ensure a sufficient Al source, we have tentatively selected 10 wt.% Al as the desired Al contents for the Fe-Ni-Cr-Al nanocoating compositions.

The candidate nanocoatings were fabricated using a magnetron-sputtering process, which previously produced nanostructured Fe-18Cr-8Ni-xAl coatings for several Al contents as part of a small business technology transfer program [28]. These coatings typically contained a columnar-grained microstructure with small amounts of pores in the as-processed condition. The grain size was in the micrometer range in the columnar grain growth direction, but was on the nanometer range (average grain size = 350–550 nm) in the transverse direction. Efforts are currently underway to further reduce the grain size by altering the deposition parameters. Computational methods applied to assess the evolution of the microstructure, the durability, and the long-term stability of these nanocoatings are highlighted in the following four sections.

Grain Growth Modeling

The expression for grain growth kinetics is generally given by [29]

$$d^2 - d_o^2 = k_g t \tag{1}$$

where d and d_o are current and initial grain diameter, respectively, t is time, and k_g is a microstructure parameter given by [25]

$$k_g = \frac{4}{3} M_{gb} \gamma_{gb} (n-6) \tag{2}$$

where M_{gb} and γ_{gb} are the mobility and energy of the grain boundaries, respectively, and *n* is the number of the grain neighbor. The grain boundary mobility is related to the diffusion coefficient (D) as given by

$$M_{gb} = \frac{\Omega D_o}{\delta_b RT} exp\left(-\frac{Q}{RT}\right) \tag{3}$$

where Ω is the molar volume, δ_b is the grain boundary thickness, D_o is the pre-exponent coefficient for diffusion, Q is the activation energy for diffusion, R is the universal gas constant, and T is absolute temperature.

The activation energy for grain growth is closely related to the activation energy for the controlling diffusive mechanisms. In Fe-based alloys, the activation energy for grain growth can vary from 91 kJ/mol to 404 kJ/mol [30]. The high value is associated with grain growth in a columnar-grained structure [30].

Eqs. (1)–(3) were utilized to compute the grain diameter as a function of anneal times for equiaxed and columnar microstructures of as-processed magnetron-sputtered Fe-18Cr-8N-10Al coating at 750°C. The results are compared against experimental data for the columnar-grained nanocoating in Fig. 4. The grain sizes of the columnar grain structure in the nanocoatings were measured on a plane normal to the columnar growth direction via Orientation Image Microscopy (OIM). The distribution of the grain diameter for the as-deposited Fe-18Cr-8Ni-10Al nanocoating is presented in the Fig. 5. The corresponding mean diameter is 1.23 μm with a standard deviation of 0.43 μm. The theoretical calculation indicates that very little grain growth occurs in the columnar microstructure at 750°C, which is in agreement with the experimental data. In contrast, substantial grain growth occurs in an equiaxed microstructure. The different grain growth kinetics is due to

the large difference in the activation energy for grain growth, which is 404 kJ/mol [30] for columnar grain structure and 245 kJ/mol for the equiaxed grain microstructure [30].

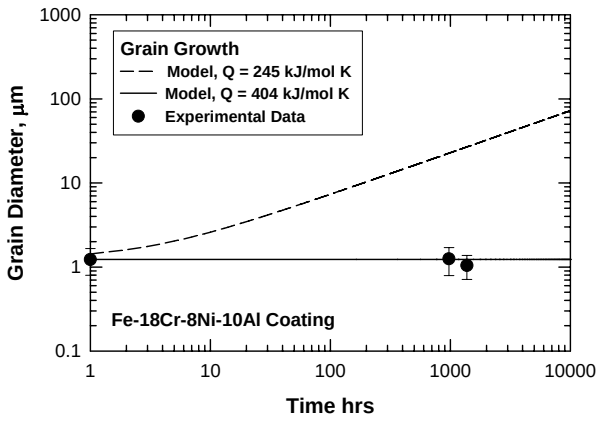

Fig. 4. Predicted grain growth kinetics using the activated energy values for equiaxed and columnar grain structures compared to experimental data for Fe-18Cr-8Ni-10Al nanocoatings with a columnar grain structure at 750°C.

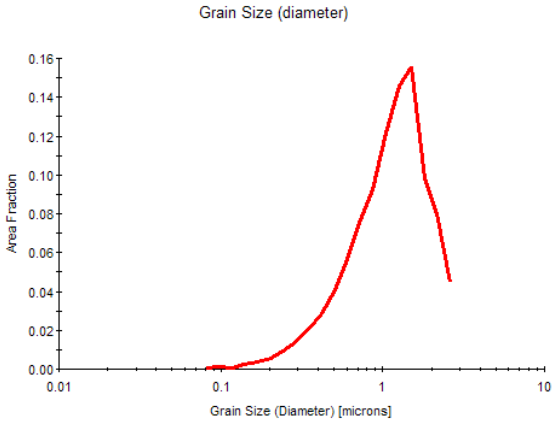

Fig. 5. Grain diameter distribution for Fe-18Cr-8Ni-10Al nanocoating in the as-coated condition.

To understand the high activation energy for the columnar grain structure, OIM was also utilized to characterize the grain orientation, and the grain boundary characters in the Fe-Cr-Ni-Al nanocoatings. Fig. 6 shows the color-coded orientation map for the as-processed Fe-18Cr-8Ni-10Al coating, which shows a random distribution of grain orientations. In contrast, the grain boundaries in the columnar structure are mostly low angle boundaries with 49% of the grain boundaries having less than a 15° misorientation angle. Fig. 7 shows that about 39% of the grain boundaries are mis-oriented by 4° or less. The distribution is fairly uniform at misorientation angles higher than 4°. The higher activation energy for grain growth in the columnar structure appears to be the result of the presence of a large fraction (about 50%) of low angle boundaries (< 15% misorientation) in the microstructure. Thus, a key to maintain a fine-grained structure that resists grain growth is to have a high population of low-angle grain boundaries in the nanocoatings. On the contrary, a high population of high-angle grain boundaries may lower the activation energy for grain growth and promote grain coarsening.

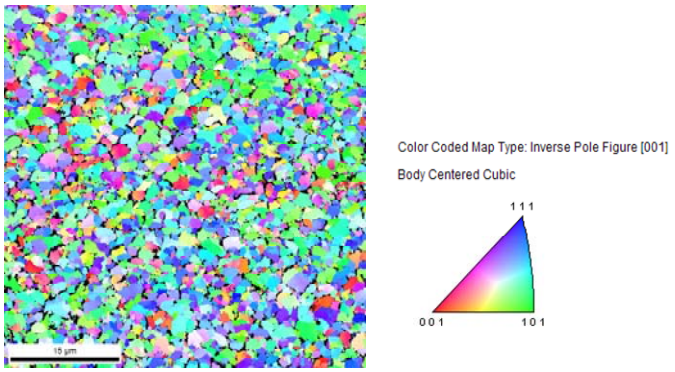

Fig. 6. Colored–coded orientation map for as-coated Fe-18Cr-8Ni-10Al nanocoating on 304 stainless steel substrate.

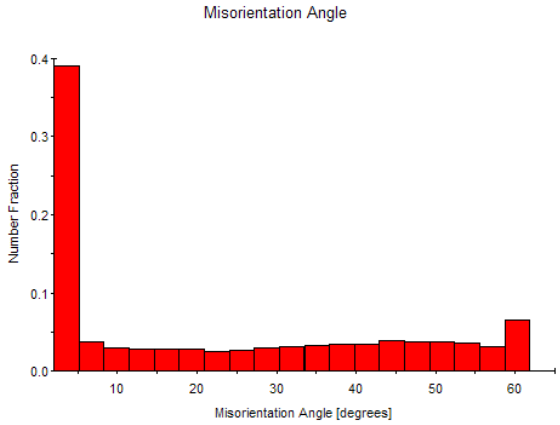

Fig. 7. Distribution of grain boundary misorientation determined by EBSD for as-coated Fe-18Cr-8Ni-10Al nanocoating on 304 stainless steel substrate.

Sintering Modeling

Connected grain boundary pores are undesirable in coatings because they promote internal oxidation by providing access of oxygen to interior grains. Experimental data indicated the presence of voids and gaps between columnar grains in the as-deposited magnetron-sputtered nanocoatings. The volume fractions of voids ranged from 10% in the as-processed condition to about 2% after cyclic oxidation at 750°C for 1500 one-hour cycles, Fig. 8. The decrease in void density was the result of sintering after high-temperature exposure.

An existing sintering model was utilized to compute the linear shrinkage rate (ΔL/L) according to [31]

$$\frac{\Delta L}{L} = \left(\frac{15a^4}{r^4} \frac{D\gamma_s}{kT} \right)^{1/3} t^{1/3} \quad (4)$$

where D is self-diffusion coefficient, γ_s is surface energy, r is grain radius, a is lattice parameter, t is time and k is Boltzmann's constant. The relative density is given in terms of the linear shrinkage rate as [31]

$$\rho = \rho_i \left[1 - \frac{\Delta L}{L} \right]^{-3} \quad (5)$$

where ρ_i is the initial density.

Using Eqs. (4) and (5), the relative density was computed as a function of time for Fe-Cr-Ni-Al nanocoatings and the results are compared against experimental data in Fig. 8. The as-coated Fe-18Cr-8Ni-10Al coating was about 90% dense, but the relative density increased with increasing times cyclic oxidation to almost 98% dense after about 1373 hours of thermal exposure at 750°C. The model prediction is in good agreement with the experimental data. The presence of pores in the coating allows oxygen penetrations and internal oxidation deep inside the nanocoatings. To eliminate oxygen penetration through connected pores, the grain boundaries pores must be eliminated or sealed off from the interior grains. The sintering model was utilized to estimate the time required to eliminate the pores. The results indicate that the initial density of the as-fabricated coating must be greater than 98% dense (i.e., less than 2% porosity) in order to eliminate all pores in less than 45 hours at 750°C. The sintering time increases to 320 hours at an initial relative density of 95%. Unlike ceramic coatings, the strain compliance of the metallic nanocoatings is not expected to decrease after sintering to achieve full density since the nanocoatings are inherently ductile.

Interface Toughness

The adhesion and spallation characteristics of the as-deposited nanocoatings were investigated by performed indentation tests using the Rockwell C indenter at 150 kg load. Indentation usually resulted in the formation of a circular indent of radius r_p and a debonded zone of radius r_d, as illustrated in Fig. 9. Results of r_p and r_d for various nanocoatings were measured and the ratios of r_d/r_p are summarized in Table 1. The ratios of r_d/r_p can be utilized to compute the interface toughness (elastic strain energy release rate) during steady-state interface debonding under indentation. Using an established procedure described by Drory and Hutchinson [32], the interface toughness values for Fe-20Cr-8Ni-10Al nanocoatings and the preliminary results are presented in Table 1. In general, the interface toughness of the Fe-20Cr-8Ni-10Al nanocoatings are in the 52–366 J/m^2 range, which are quite high compared to typical values of less than 1–10 J/m^2 for brittle coatings [33], but are consistent with 14–215 J/m^2 for ductile W/Cu coatings [33].

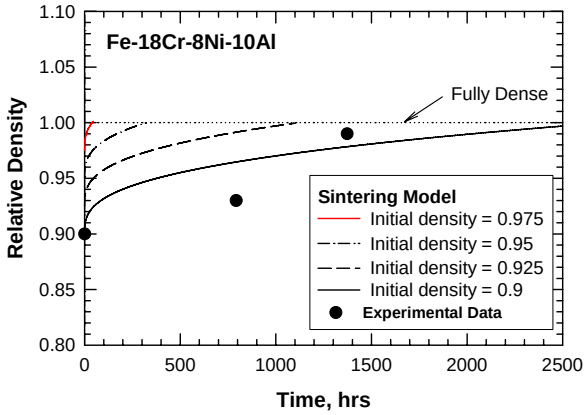

Fig. 8. Theoretical relative density based on the sintering model compared to experimental data of Fe-18Cr-8Ni-10Al coating on Fe-18Cr-8Ni substrate. The initial relative density of the as-processed coating must be greater than 98% in order to achieve the full density in less than 45 hours of exposure at 750°C.

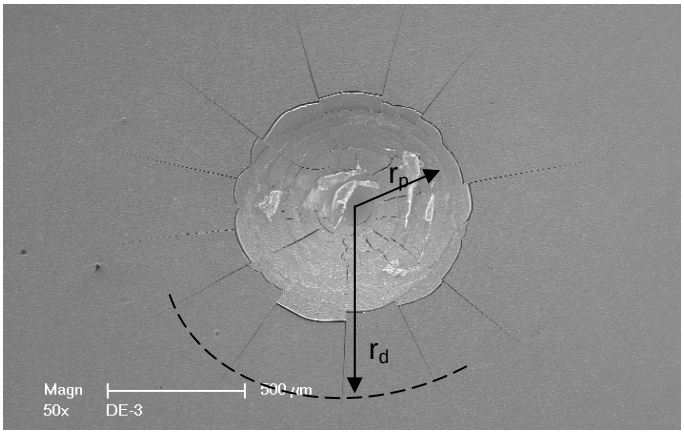

Fig. 9. Rockwell C indentation on a Fe-20Cr-8Ni-10Al nanocoating on Fe-18Cr-8Ni substrate resulted in a circular indent of radius r_p and a cracked/debonded zone of radius r_d. The ratio of r_d/r_p was utilized to deduce the elastic strain energy release rate or interface toughness during steady-state interface debonding using the procedure developed by Drory and Hutchinson [32].

Table 1. Ratios of r_d/r_p and interface toughness of Fe-20Cr-8Ni-10Al nanocoatings processed under various voltage and ion bombardment conditions.

Nanocoating	r_d/r_p	Γ_{ss}, J/m^2
DE-1	1.861 ± 0.230	109.6 ± 65.7
DE-2	1.438 ± 0.083	365.5 ± 96.2
DE-3	1.832 ± 0.084	104.7 ± 26.8
DE-4	2.086 ± 0.146	52.1 ± 21.7
DE-5	1.496 ± 0.031	294.6 ± 29.9

Interdiffusion between Coating and Substrate

The microstructural stability of a coating on a particular substrate during long-term high-temperature exposures was evaluated by performing interdiffusion computation treating the coating and the substrate as a diffusion couple. As illustrated in Fig. 10, the coating was taken to be 30 μm on top of a substrate that is considered to be much thicker than the coating. For the purpose of minimizing the computation times, the substrate thickness was taken to be 150 μm. Interdiffusion computation was performed using DICTRA 24 [3] with TCFE5 [2] thermodynamic database and MOB2 mobility database. In these computations, only interdiffusion diffusion due to chemical gradients was considered, but outward diffusion due to oxidation was ignored.

Interdiffusion of Al, Cr, and Ni were computed for Fe-18Cr-8Ni-10Al coating on Fe-18Cr-8Ni (304SS) substrate at 750°C for exposure times of 625, 825, 1250, 2500, and 8760 hrs. Figs. 11(a), (b), and (c) show the concentration profiles for Al, Cr, and Ni, respectively. The initial Al concentration (dotted line) in the coating was 10 wt.%. Inward diffusion of Al occurred fairly rapidly and the Al concentration deceased to about 4.1 wt.% after 625 hrs and to 2 wt.% after 8760 hrs (1 yr). Like Al, Cr and Ni also diffused inwardly into the substrate, but their concentration files are more complex, as shown in Figs. 11(b) and (c). The coating contains mostly α (bcc) with about 10–20 mole % γ (fcc). In contrast, the substrate is predominantly γ (fcc) but the mole fraction of α (bcc) phase increases with time as more Al diffuses inwardly into the substrate.

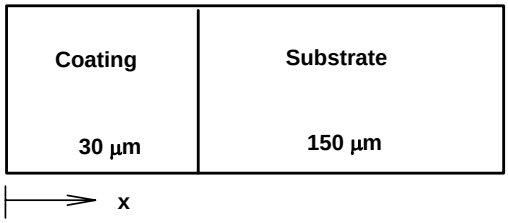

Fig. 10. Diffusion couple used in the interdiffusion computation using DICTRA.

For Fe-25Cr-40Ni-10Al on Fe-18Cr-8Ni at 750°C, inward diffusion of Al, Cr, and Ni into the substrate after 825 hrs of exposure is presented in Figs. 12(a), (b), and (c), respectively. As shown in Fig. 12(a), there is some inward diffusion of Al into the substrate, but the rate of Al loss to the substrate is considerably lower compared to coatings with lower Cr and Ni contents. In addition, Figs. 12(b) and (c) indicate that the Cr and Ni loss to the substrate is also lower. The phase fraction results indicate that the formation of an fcc layer at the coating/substrate interface. This fcc layer appears to act as a diffusion barrier that limits the inward diffusion of Al and Cr into the substrate at 750°C.

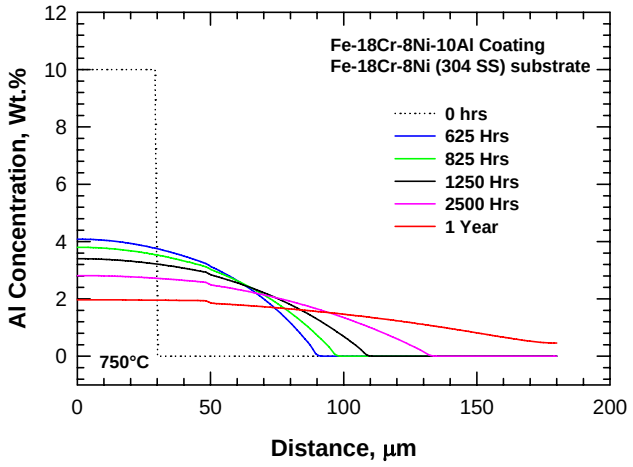

(a)

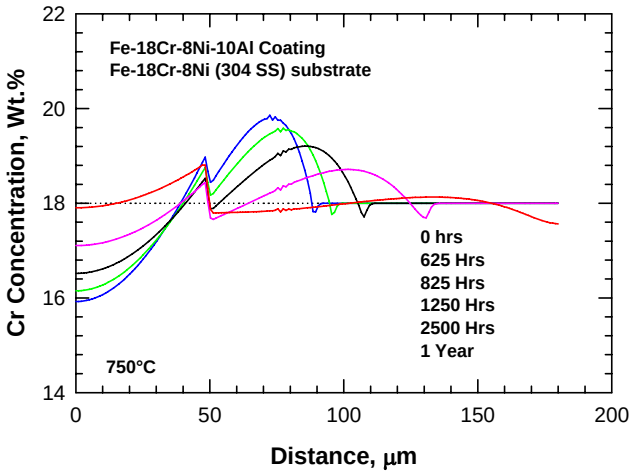

(b)

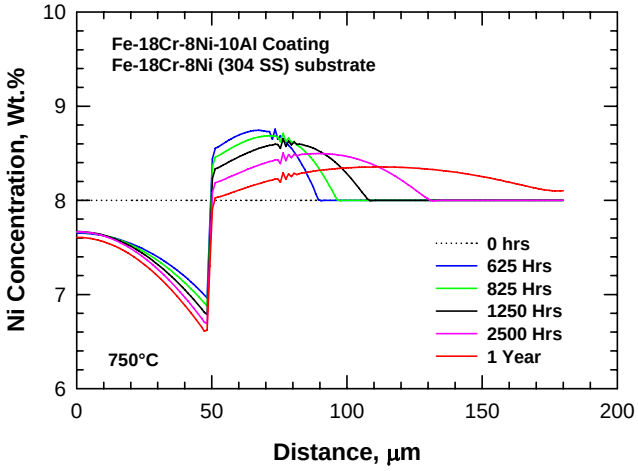

(c)

Fig. 11. Computed concentration profiles for Fe-18Cr-8Ni-10Al coating on Fe-18Cr-8Ni substrate after various times of exposure at 750°C: (a) Al distribution, (b) Cr distribution, and (c) Ni distribution.

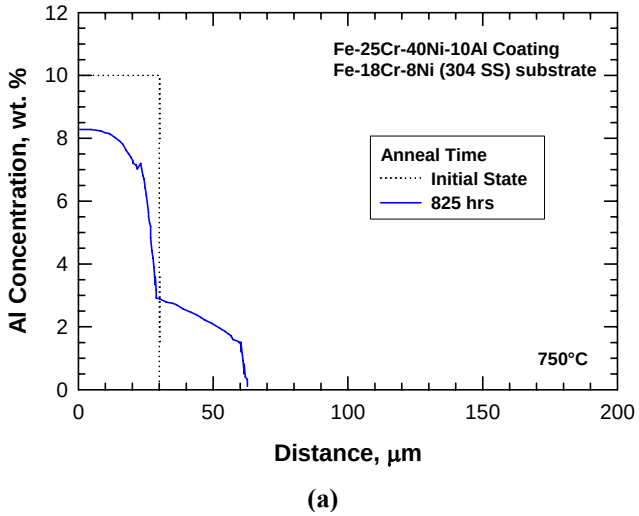

(a)

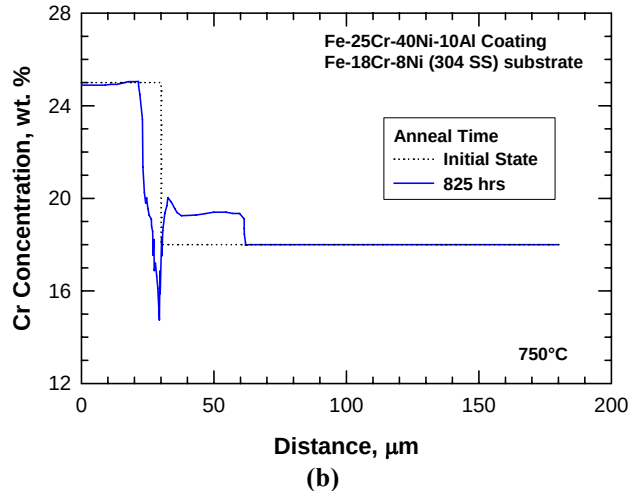

(b)

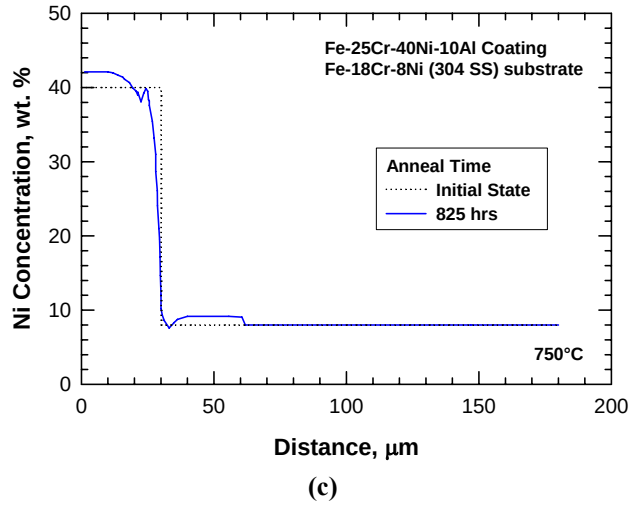

(c)

Fig. 12. Computed concentration profiles for Fe-25Cr-40Ni-10Al coating on Fe-18Cr-8Ni (304 SS) substrate after 825 hours at 750°C: (a) Al concentration, (b) Cr concentration, and (c) Ni concentration.

Comparison of Model Computation Against Experiment

Limited efforts were also initiated to compare the theoretical computations against experimental data of Fe-Cr-Ni-Al coatings produced in a small business technology transfer program [28]. In this program, Fe-18Cr-8Ni-xAl coatings were investigated at several Al contents. Without Al additions, Fe-18Cr-8Ni (304 SS) coating showed the presence of σ phase in the as-deposited and thermally exposed conditions. The microstructure was predominantly bcc ferrite and σ phases, as shown in Fig. 13(a). The σ phase was suppressed by an Al addition as small as 3 wt.% Al. At 10 wt.% Al, Fe-18Cr-8Ni-10Al contained mostly ferrite (bcc) with small amounts of austenite (fcc) after 990 one-hour thermal cycles at a peak temperature of 750°C, as shown in Fig. 13(b). These experimental findings are in agreement with phase-diagram computations obtained via Thermo-Calc®.

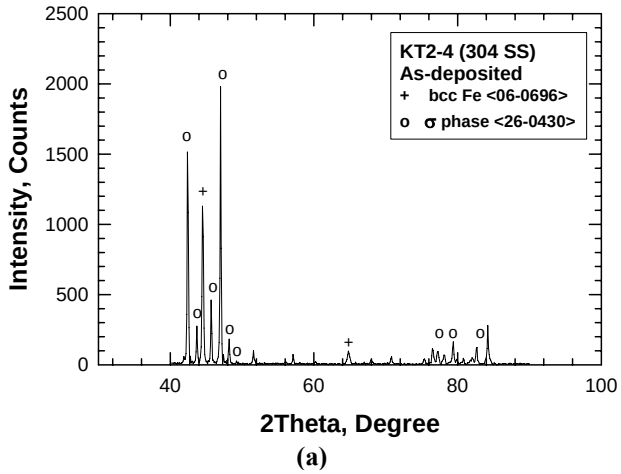

(a)

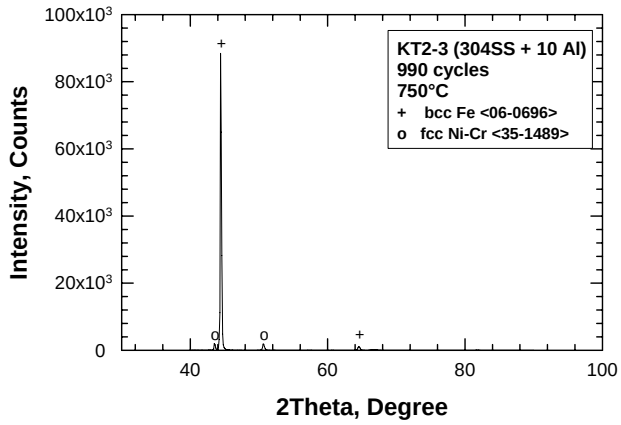

(b)

Fig. 13. XRD patterns of Fe-18Cr-8Ni (304SS) and Fe-18Cr-8Ni-10Al (304SS+10Al) show the presence of σ phase without Al addition in 304 SS and the absence of σ phase in Fe-18Cr-8Ni-10Al with 10 wt.% Al addition. These specimens have been subjected to 990 one-hour thermal cycles at a peak temperature of 750°C.

The computed concentration profiles of Al, Cr, and Ni based on inward diffusion are compared against experimental data from cyclic oxidation specimens of Fe-18Cr-8Ni-10Al on Fe-18Cr-8Ni (304 SS) substrate tested at a maximum temperature of 750°C. All chemical compositions were determined by energy-dispersive X-ray spectroscopy (EDXS). Fig. 14(a) shows a comparison of the predicted and measured Al profiles in the coating and in the substrate after 825 hrs of thermal exposure. In general, the predicted Al profile is in good agreement with the observed profile. The Al content in the coating is predicted to decrease from 10 wt.% to 3.7 wt.% in the coating. The depth of the interdiffusion zone is predicted to be about 70 μm. Both predictions are in excellent agreement with the experimental data as shown in Fig. 14(a). The corresponding concentration profiles for Cr and Ni are compared against experimental data in Figs. 14(b) and (c), respectively. For both Cr and Ni, the complex profiles detailed by the computations could not be verified by the experimental data. On the other hand, the model predictions of minimal Cr and Ni loss to the substrate by inward diffusion are confirmed in general.

DISCUSSION

The oxidation resistance of an Fe-Cr-Ni-Al coating depends on the formation of a continuous alumina layer on the coating surface. A critical Al content in excess of 3.5 wt.% to 5 wt.% is typically required for continuous alumina formation with the critical value of the Al content deceasing with increasing grain sizes in the coating [15, 23]. The critical Al content is further decreased to about 2.5 wt.% in micro-alloyed Fe-Ni-Cr-Al alloys by eliminating Ti or V additions [24–26]. An estimate of coating life due to Al loss by inward diffusion can thus be made by using an Al content of 3.5 wt.% as the minimum amount required in an oxidation-resistant Fe-Cr-Ni-Al nanocoating [15, 23]. For Fe-18Cr-8Ni-10Al on Fe-18Cr-8Ni, the Al content in the coating decreases to less than 3.5 wt.% after about 1250 hrs at 750°C due to inward diffusion, Fig. 11(a). For Fe-25Cr-40Ni-10Al on Fe-18Cr-8Ni, the time to the critical Al content is much larger than 825 hrs due to the presence of an fcc layer, which acts as a diffusion barrier, at the coating/ substrate interface. This finding is consistent with a previous study, which showed that for aluminide coatings on Fe-based substrates, an austenitic substrate acts as a diffusion barrier to the ingress of Al and slows down the interdiffusion [34].

The formation of an interdiffusion barrier layer has also been observed in aluminide coatings on Fe-based alloys [34, 35]. In the case of aluminide coatings, the interdiffusion barrier layer is comprised of a two-phase microstructure containing bcc ferrites and B2 nickel aluminides [34] or iron aluminides [35]. Thus, the type of interdiffusion barrier layer formed at the coating/substrate depends on both the coating and substrate.

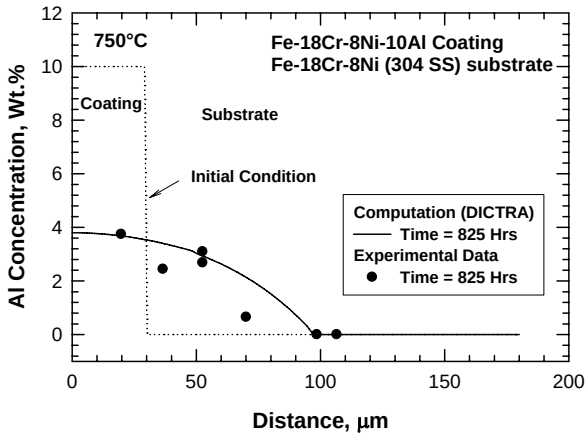

(a)

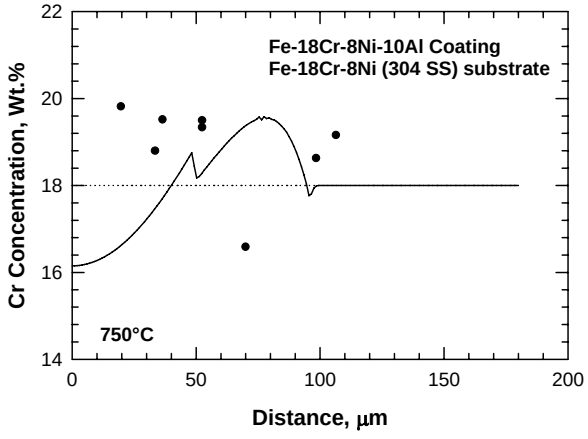

(b)

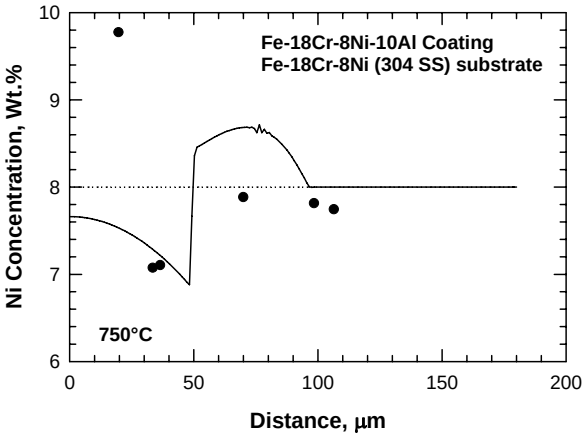

(c)

Fig. 14. Calculated concentration profiles compared against experimental data for Fe-18Cr-8Ni-10Al coating on Fe-18Cr-8Ni substrate after 825 hrs at 750°C: (a) Al content, (b) Cr content, and (c) Ni content.

The loss of Al from Fe-Cr-Ni-Al coatings may render them susceptible to excessive oxidation resulting from difficulties in forming a continuous alumina film formation. On the other hand, the presence of a high Cr content in the coatings may provide resistance against oxidation and corrosion. Thus, it is worthwhile to compare the Cr concentration profile against the critical content for chromia formation. The corrosion resistance of an Fe-Cr-Ni coating depends on the formation of a continuous chromia layer on the coating surface. A critical Cr content in excess of 16 wt.% is typically required for continuous chromia formation [36], but the critical Cr content also depends on the Ni content [37]. For resistance against type II corrosion, the critical Cr content in excess of 25 wt.% is required [38, 39]. An estimate of coating life due to Cr loss by inward diffusion can be made by using a Cr content of 16 wt.% (or 25 wt.%) as the minimum amount required in a corrosion-resistant Fe-Cr-Ni coating. For Fe-18Cr-8Ni-10Al on Fe-18Cr-8Ni, the critical Cr content of 16 wt.% for Cr_2O_3 formation and reformation is met in this coating/substrate system over the time periods considered. For Fe-25Cr-40Ni-10Al on Fe-18Cr-8Ni, a Cr content of 16 wt.% can be maintained in the coating after 825 hrs because of the formation of an fcc phase diffusion barrier at the coating/substrate interface, Fig. 12(b). Additional computations to longer time periods are required to pinpoint the oxidation or corrosion life of this coating.

CONCLUSIONS

The conclusions reached as the results of the computational modeling efforts are as follows:

1. Pseudo-ternary phase diagrams computed via Thermo-Calc® software provides detailed information on the constituent phases in Fe-Cr-Ni-Al alloys at various temperatures.

2. The formation of sigma phase in Fe-Cr-Ni-Al alloys is suppressed for Al contents in excess of 4 wt.% for temperatures in the range of 600 to 1200 K.

3. Grain growth modeling indicated that the columnar-grained structure observed in Fe-18Cr-8Ni-(4-10)Al nanocoatings is stable and resistant to grain growth because of a high activation energy for grain growth due to a low grain boundary energy resulting from a high percentage of low-angle grain boundaries.

4. Sintering modeling indicated that the initial relative density of the as-processed coating must be greater than 98% in order to achieve full density in less than 2 days of thermal exposure at 750°C.

5. Interface toughness computation indicated that Fe-Cr-Ni-Al nanocoatings produced by magnetron sputtering at SwRI exhibit high interface toughness in the range of 52–366 J/m^2.

6. Interdiffusion modeling using the DICTRA software package indicated that inward diffusion results in Al and Cr losses from the nanocoating to the substrate during thermal exposure at 750°C.

ACKNOWLEGMENTS

This work was supported by the Department of Energy through Contract No. DE-FC26-07NT439096 and monitored by Ms. Patricia Rawls, Program Manager. The clerical assistance of Ms. L. Mesa in the preparation of the manuscript is acknowledged.

REFERENCES

1. A. B. Thermo-Calc® Software, Thermo-Calc for Windows Version 4, Thermo-Calc Software AB, Stockholm, 2007.

2. A. B. Thermo-Calc® Software, TCFE5, Version 5, Thermo-Calc Software AB, Stockholm, 2007.

3. A. B. Thermo-Calc Software, DICTRA, Version 24, Thermo-Calc Software AB, Stockholm, 2007; Version 25, 2008.

4. F-H. Wang, "The Effect of Nanocrystallization on the Selective Oxidation and Adhesion of Al_2O_3 Scales," *Oxidation of Metals,* Vol. 48 (1997) 215–223.

5. Z-Y. Liu, W. Gao, K. L. Dahm, and F-H. Wang, "Oxidation Behaviour of Sputter-Deposited Ni-Cr-Al Micro-Crystalline Coatings," *Acta Mater.,* Vol. 46 (1998) 1691–1700.

6. Z-Y. Liu and W. Gao, "Oxidation Behaviours of Microcrystalline Ni-Cr-Al Alloy Coatings at 900°C," *Scripta Mater.,* Vol. 38 (1998) 877–885.

7. G-F. Chen and H-Y. Lou, "The Effect of Nanocrystallization on the Oxidation Resistance of Ni-5Cr-5Al Alloy," *Scripta. Mater.,* Vol. 41 (1999) 883–887.

8. G-F. Chen and H-Y. Lou, "Oxidation Behavior of Sputtered Ni-3Cr-20 Al Nanocrystalline Coating," *Mater. Sci. Eng. A,* Vol. A271 (1999) 360–365.

9. Z-Y. Liu, W. Gao, K. L. Dahm, and F-H. Wang, "Improved Oxide Spallation Resistance of Microcrystalline Ni-Cr-Al Coatings," *Oxidation of Metals.,* Vol. 50 (1998) 51–69.

10. G. Chen and H. Lou, "Oxidation Behavior of Sputtered Ni-Cr-Al-Ti Nanocrystalline Coating," *Surf. Coat. Technol.,* Vol. 123 (2000) 92–96.

11. G-F. Chen and H-Y Lou, "Effect of Nanocrystallization on the Oxidation Behavior of a Ni-8Cr-3.5 Al Alloy," *Oxidation of Metals,* Vol. 54 (2000) 155–162.

12. L. Ajdelsztajn, F. Tang, G. E. Kim, V. Provenzano, and J. M. Shoenung, "Synthesis and Oxidation Behavior of Nanocrystalline MCrAlY Bond Coats," *J. Thermal Spray Technol.,* Vol. 14 (2005) 23–30.

13. N. S. Cheruvu, "Nanostructured Coatings by Pulsed Plasma Processing for Alloys used in Coal-fired Environments," Department of Energy, Small Business Technology Transfer (STTR) Program, DE-FG02-5ER 86249, SwRI 4th Quarter**ly** Report to Karta Technologies, February 2008.

14. Z-Y. Liu, W. Gao, and M-S. Li, "Cyclic Oxidation of Sputter-Deposited Nanocrystalline Fe-Cr-Ni-Al Alloy Coatings, *Oxidation of Metals,* Vol. 51 (1999) 403–419.

15. Z. Liu, W. Gao, and Y. He, "Oxidation Behaviour of Nanocrystaliine Fe-Ni-Cr-Al Alloy Coatings," *Materials Science and Technology,* Vol. 15 (1999) 1447–1450.

16. Y. He, H. Pang, H. Qi, D. Wang, Z. Li, and W. Gao, "Micro-crystalline Fe-Cr-Ni-Al-Y_2O_3 ODS Alloy Coatings Produced by High Frequency Electric-spaak Deposition," *Materials Science and Engineering,* Vol. A334 (2002) 179–186.

17. I. G. Wright, P. A. Pint, L. M. Hall, and P. F. Tortorelli, in *Lifetimes Modeling of High-Temperature Corrosion Processes,* M. Schutze, W. J. Quadakkers, and J. R. Nicholls, eds., EFC Publications No. 34, Maney Publishing, 2001, pp. 339–358.

18. J. T. Murphy, J. R. Regina, R. M. Deacon, J. N. DuPont, and A.R. Marder, Proceedings of the Nineteenth Annual Conference on Fossil Energy Materials, May 9-11, 2005, Knoxville, Tennessee.

19. J. C. Pivin, D. Delaunay, C. Roques-Carmes, A. M. Huntz, and P. Lacombe, *Corrosion Science,* Vol. 20 (1980) 351–373.

20. T. T. Huang, R. Richter, Y. L.Chang, and E. Pfender, *Metall. Trans. A.,* Vol. 16A (1985) 2051–2059.

21. M. Karaminezhaad, E. Kordzadeh, and M. R. Bateni, *J. of Corrosion Sci. and Eng.,* Vol. 7, Paper 4, 2004.

22. S. Yamada, H. Tadashi, Y. Kawamura, and T. Saburi, *J. of High-Temperature Society,* Vol. 26, No. 3 (2000) 131–137 (in Japanese).

23. W. Gao, Z. Liu, and Z. Li, *Advanced Materials*, Vol. 13, No. 12-13, 2001, pp. 1001–1004.

24. B. A. Pint, R. Peraldi, and P. J. Maziasz, "The Use of Model Alloys to Develop Corrosion-Resistant Stainless Steels," *Materials Science Forum,* Vol. 461-464 (2004) 815–822.

25. M. P. Brady, Y. Yamamoto, M. L. Santella, and B. A. Pint, "Effects of Minor Alloy Additions and Oxidation Temperature on Protective Alumina Scale Formation in Creep-Resistant Austenitic Stainless Steels," *Scripta Materialia,* Vol. 57 (2007) 1117–1120.

26. Y. Yamamoto, M. P. Brady, Z. P. Lu, P. J. Maziasz, C. T. Liu, B. A. Pint, K. L. More, H. M. Meyer, and E. A. Payzant, "Creep-Resistant Al_2O_3-forming Austenitic Stainless Steels," *Science*, Vol. 316 (2007) 433–436.

27. B. A. Pint, Y. Zhang, L. R. Walker, and I. G. Wright," Long-term Performance of Aluminide Coatings on Fe-based Alloys," *Surface & Coatings Technology*, Vol. 202, (2007) 637–642.

28. "Nanostructured Coatings by Pulsed Plasma Processing for Alloys used in Coal-fired Environments," Department of Energy, Small Business Technology Transfer (STTR) Program, DE-FG02-5ER 86249.

29. M. Hillert, *Acta Metall*, Vol. 13 (1965) 227–238.

30. Y. Sidor, F. Kovac, and V. Petrychka, *Metabk,* Vol. 44, No. 3, 2005, pp. 169–174.

31. D. L. Johnson and I. B. Cutler, *J. Am. Ceramic Soc.,* Vol. 46, No. 11, 1963, pp. 541–545.

32. M. D. Drory and J. W. Hutchinson, *Proc. R. Soc., London A,* Vol. 452 (1996) 2319–2341.

33. A. A. Volinsky, N. R. Moody, and W. W. Berberich, *Acta Mater.,* Vol. 50 (2002) 441–466.

34. N. V. Bangaru and R. C. Krutenat, "Diffusion Coatings of Steels: Formation Mechanism and Microstructure of Aluminized Heat-Resistant Stainless Steels," *J. Vac. Sci. Technology*, Vol. 2 (1984) 806–815.

35. Y. Zhang, A. P. Liu, and B. A. Pint, "Interdiffusional Degradatino of Oxidation-Resistant Aluminide Coatings on Fe-based Alloys," *Materials and Corrosion*, Vol. 58 (2007) 751–761.

36. H. E. Evans, A. T. Donaldson, and T. C. Gilmour, *Oxidation of Metals,* Vol. 52, No. 5/6, 1999, pp. 379–402.

37. R. Peraldi and B. A Pint, *Oxidation of Metals,* Vol. 61, No. 5/6, 2004, pp. 463–483.

38. P. Castello, V. Guttmann, N. Farr, and G. Smith, *Materials and Corrosion,* Vol. 51 (2000) 786–790.

39. H. Hack and G. Stanko, Presented at the 31st Int. Technical Conference on Coal Utilization & Fuel Systems, May 1-26, 2006, Sand Key Island, Florida.